Gene Silencing by Gold Nanoshell-Mediated Delivery and Laser-Triggered Release of Antisense Oligonucleotide and siRNA

Ryan Huschka,[†] Aoune Barhoumi,[†] Qing Liu,[¶] Jack A. Roth,[¶] Lin Ji,[¶] and Naomi J. Halas[†,‡,§,⊥,*]

[†]Department of Chemistry, [‡]Department of Electrical and Computer Engineering, [§]Department of Physics and Astronomy and [⊥]Department of Bioengineering, Rice University, 6100 Main Street, Houston, Texas 77005, United States, and [¶]Department of Thoracic and Cardiovascular Surgery, The University of Texas MD Anderson Cancer Center, 1515 Holcombe Boulevard, Houston, Texas 77030, United States

ABSTRACT RNA interference (RNAi)—using antisense DNA or RNA oligonucleotides to silence activity of a specific pathogenic gene transcript and reduce expression of the encoded protein—is very useful in dissecting genetic function and holds significant promise as a molecular therapeutic. A major obstacle in achieving gene silencing with RNAi technology is the systemic delivery of therapeutic oligonucleotides. Here we demonstrate an engineered gold nanoshell (NS)-based therapeutic oligonucleotide delivery vehicle, designed to release its cargo on demand upon illumination with a near-infrared (NIR) laser. A poly-L-lysine peptide (PLL) epilayer covalently attached to the NS surface (NS-PLL) is used to capture intact, single-stranded antisense DNA oligonucleotides, or alternatively, double-stranded short-interfering RNA (siRNA) molecules. Controlled release of the captured therapeutic oligonucleotides in each case is accomplished by continuous wave NIR laser irradiation at 800 nm, near the resonance wavelength of the nanoshell. Fluorescently tagged oligonucleotides were used to monitor the time-dependent release process and light-triggered endosomal release. A green fluorescent protein (GFP)-expressing human lung cancer H1299 cell line was used to determine cellular uptake and gene silencing mediated by the NS-PLL carrying GFP gene-specific single-stranded DNA antisense oligonucleotide (AON-GFP), or a double-stranded siRNA (siRNA-GFP), *in vitro*. Light-triggered delivery resulted in ~47% and ~49% downregulation of the targeted GFP expression by AON-GFP and siRNA-GFP, respectively. Cytotoxicity induced by both the NS-PLL delivery vector and by laser irradiation is minimal, as demonstrated by a XTT cell proliferation assay.

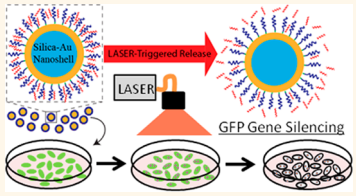

KEYWORDS: plasmon · nanoshell · antisense oligonucleotide · siRNA · gene therapy · controlled drug release · poly-L-lysine

RNAi—the use of short-interfering RNA (siRNA) or antisense DNA oligonucleotides to silence or interrupt the activity of specific genes and downregulate expression of their encoded proteins—has proved to be very useful in dissecting genetic function.[1] This approach holds considerable promise for the development of a new class of molecular therapeutic drugs that interferes with disease-causing or -promoting genes, particularly those that encode so-called "nondruggable" targets not amenable to conventional therapeutics.[2] However, the main obstacle to achieving gene silencing *in vivo* by RNAi technologies is delivery of therapeutic siRNAs or antisense oligonucleotides, currently becoming a major topic in cancer therapy. This goal faces many challenges, such as the direction of specific gene targets to the appropriate tissue and cell types at safe and effective dosages, and maintenance of oligonucleotide stability in circulation. Strategies for enhancement of cellular uptake and methods for monitoring distribution and therapeutic efficacy are also needed.[2−5] Overcoming these obstacles requires new delivery vehicles and targeting approaches. Lipid and polymer-based vehicles for administration of siRNA have been developed and tested for delivery to lung, liver, and other local tumors in animal models, including nonhuman primate.[2,3,6] These RNA or DNA oligonucleotide delivery carriers present a variety of potential problems to the patient: toxicity, immune and inflammatory responses, and gene control and targeting issues.[2−7] Realizing the full potential of RNAi-based molecular therapeutics requires new strategies[8−18] to substantially improve delivery efficiency, toxicity profiles, monitoring techniques, and pharmacological and therapeutic efficacy.

Gold nanoparticles show potential to offer "on-demand" release in response to optical laser excitation due to their plasmon resonance, the collective oscillation of their electrons.[19−21] Recently, two strategies for

* Address correspondence to halas@rice.edu.

Received for review March 14, 2012 and accepted August 4, 2012.

Published online August 04, 2012
10.1021/nn301135w

light-triggered release have been investigated. One strategy consists of covalently attaching the gene therapeutic to the gold surface. Upon irradiation with femtosecond laser pulses, the nanoparticles either break apart or reshape into small gold nanoparticles, breaking the covalent bond and releasing the gene therapeutic.[13,18,19,22,23] The second strategy consists of covalently attaching a "carrier" molecule to the gold surface and then loading the "cargo" gene therapeutic molecule onto the carrier molecule, typically by weaker, noncovalent bonds. Upon laser illumination, the nanoparticle absorbs energy, which modulates the attraction between the carrier and cargo molecules either thermally or nonthermally, resulting in release of the therapeutic entity.[24−27] While both strategies show promise, the second strategy may be advantageous due to the relatively low laser power densities and short irradiation times required to release the therapeutic cargo.

Gold (Au) nanoshells (NSs), composed of a spherical silica core coated with a thin Au shell, show excellent potential for offering "on-demand" release in response to optical excitation. The plasmon resonance of Au nanoshells can be tuned from the visible region into the near-infrared (NIR) by changing the core size and the thickness of the gold shell.[28] The NIR resonance of NSs enables biomedical applications because the nanoshell can be easily fabricated to maximally absorb in the NIR "water window", where bodily tissue is maximally transparent.[29] Au nanoshells have been used extensively in biomedical applications, including photothermal cancer therapy.[30−34] Additionally, Au possesses a very well-established Au-thiol bond chemistry that allows easy functionalization of the nanoshell surface with a wide variety of ligands and targeting moieties.[16,35]

Recently we demonstrated resonant light-induced release of single-stranded DNA (ssDNA) from Au nanoshells.[20,36,37] A monolayer of double-stranded DNA (dsDNA) was attached to the nanoshell surface *via* a thiol modification on the 5′ end of a complementary, carrier sequence, while a therapeutically antisense sequence to be released was hybridized to its carrier complement *via* Watson−Crick base-pairing. Continuous wave laser radiation at 800 nm released the nonthiolated DNA strand from the nanoshell surface. In this previous work, the thiolated DNA sequence is the carrier molecule that holds the therapeutic ssDNA cargo. By monitoring the light-triggered molecular release as a function of ambient solution temperature, it was apparent that both a thermal and a nonthermal mechanism were responsible for the release. Significant ssDNA release was measured for ambient solution temperatures well below the DNA melting (dehybridization) temperature in this system, with additional release occurring at and above the DNA melting temperature. This rudimentary light-triggered delivery system is limited to the release of single-stranded oligonucleotides. However, its demonstration suggests that noncovalent binding may be used to create a more general "carrier" platform capable of delivering a range of different types of oligonucleotide therapies upon NIR irradiation, where one would also anticipate that the molecular cargo release response would be facilitated by both a thermal and a nonthermal release mechanism.

Cationic poly-L-lysine peptides are a promising oligonucleotide carrier. poly-L-lysine has been used extensively as a transfection reagent for gene therapeutics.[38−40] Due to the fact that it is positively charged at physiological pH, poly-L-lysine associates electrostatically with the negatively charged phosphate backbone of antisense DNA or siRNA oligonucleotides. In addition, the poly-L-lysine can protect the synthetic oligonucleotide-based molecular therapeutics from enzymatic degradation by nucleases during transport and can increase cellular uptake.[39,41]

In this study we developed an NS-based antisense RNAi oligonucleotide delivery system. This nanotherapeutic delivery vector consists of an Au nanoshell functionalized with a cationic poly-L-lysine (PLL) peptide (cysteine(C)−tyrosine(Y)−serine(S)−lysine$(K)_{50}$) carrier arm for electrostatic capture of intact, negatively charged therapeutic RNAi oligonucleotides. The thiol side chain on the cysteine amino acid is utilitzed to attach the peptide to the gold surface, the tyrosine and the serine amino acid serve as spacer and the 50 lysine amino acids result in a net positive charge. To demonstrate the general utility of this delivery system, two types of RNAi cargoes, single-stranded antisense DNA oligonucleotides (ssDNA) and double-stranded siRNA are alternatively loaded onto the nanoshell-poly-L-lysine (NS-PLL) vector. Laser irradiation of the NS-PLL delivery vector controllably releases the therapeutic oligonucleotides at a controlled time point (Scheme 1). We investigated the release profile of the ssDNA and quantified the number of ssDNA molecules released by both thermal and laser-induced treatment in solution and in living cells *in vitro*. Fluorescently tagged ssDNA was used to investigate intracellular light-triggered release and endosome rupture. The NS-PLL vector was also used to deliver either the GFP gene-specific antisense DNA oligonucleotide (AON-GFP), or siRNA (siGFP), to evaluate cellular uptake and gene silencing potential of this approach in GFP-expressing H1299 lung cancer cells *in vitro*.

RESULTS AND DISCUSSION

Nanoshell Synthesis and Poly-L-lysine Functionalization. Au nanoshells were synthesized according to a previously published method.[28] The dimensions of the silica core and the Au shell ($[r_1, r_2]$ = [60, 82] nm) were designed so that the peak plasmon resonance in an aqueous

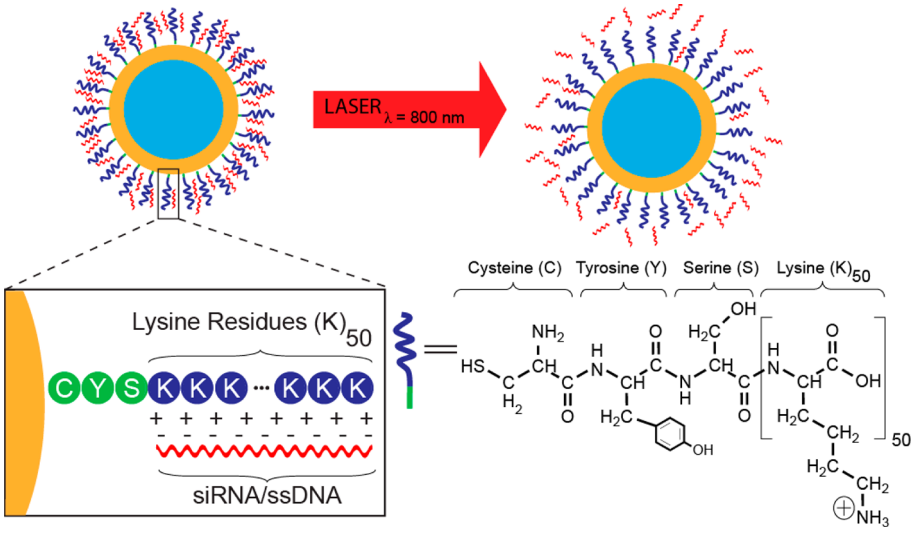

Scheme 1. Au-nanoshell poly-L-lysine (NS-PLL)-based therapeutic RNAi oligonucleotide delivery system. The negatively charged phosphate backbone of the siRNA/ssDNA (red) is electrostatically attached to the cationic peptide (blue), which consists of 1 cysteine, 1 tyrosine, 1 serine, and 50 lysine amino acids. Upon laser irradiation, the siRNA/ssDNA is released.

suspension occurred at 800 nm, corresponding to the laser excitation wavelength used in this experiment (Figure S1, Supporting Information). The PLL peptide (cysteine (C)−tyrosine(Y)−serine(S)−lysine$(K)_{50}$) was custom synthesized (Biomatik USA, LLC), received as a lyophilized powder, and resuspended in Milli-Q water. An excess of the PLL peptide (see Methods section) was added to a solution of nanoshells. This solution was allowed to incubate for 24 h on a rocker at room temperature. The excess PLL peptide was removed by centrifugation and resuspended in Milli-Q water. ζ-Potential measurements confirmed PLL attachment (Table 3). The PLL peptide mechanism of attachment to Au nanoshells could consist of both Au-thiol binding through the cysteine amino acid and electrostatic binding between the positively charged PLL peptide and the negatively charged Au nanoshell surface.

Thermal and Light-Triggered Release of ssDNA. Light-triggered release of antisense DNA oligonucleotides (ssDNA) was investigated using three types of fluorescently tagged ssDNAs (Table 1): (i) an 18-base sequence that was chemically unmodified (short ssDNA), (ii) an 18-base ssDNA with sequence identical to the first except chemically modified with phosphorothioate (phosphorothioate-modified short ssDNA), and (iii) a 50-base ssDNA that was chemically unmodified (long ssDNA). Oligonucleotides with phosphorothioate linkages were chosen because this chemical modification minimizes enzymatic degradation by nucleases and increases antisense oligonucleotide activity.[42] These chemically modified oligonucleotides have been used extensively both *in vitro* and *in vivo*.[42−44] Because the phosphorothioate-modified short DNA sequence is used to downregulate GFP *in vitro*, we needed to ensure that it could be released from the vector in a manner similar to the nonmodified DNA. The short and long ssDNA were designed to investigate the correlation between sequence length and releasing profile.

TABLE 1. ssDNA and siRNA Sequences Used in This Study

short ssDNA	5′-GAGCTGCACGCTGCCGTC-3′
phosphorothioate-modified short ssDNA	5′-G*A*G*C*T*G*C*A*C*G*C*T*G*C*C*G*T*C-3′[a]
long ssDNA	5′-GCGGCAATCAGGTTGACCGTACATCATAGCAGG-CTAGGTTGGTCGCAGTC-3′
siRNA antisense strand	5′-AUAGACGUUGUGGCUGUUGUA-3′
siRNA sense strand	5′-UACAACAGCCACAACGUCUAU-3′

[a] The asterisks denote phosphorothioate modification.

For the thermally induced release of the three fluorescently tagged ssDNAs from the NS-PLL delivery vector, the solution is slowly heated in a temperature-controlled water bath (Figure 1). Light-induced release was measured with respect to the ambient temperature of the solution, which increases upon laser irradiation due to photothermal heating by the irradiated nanoshells.

For all three ssDNAs studied, the laser irradiation resulted in ssDNA release at lower solution temperatures compared to thermal release (Figure 1). The release of some of the ssDNAs was detected immediately upon laser irradiation (Figure 1, black squares). In contrast, for the thermal treatment (red dots), the ssDNA was released gradually as the solution temperature was increased. For light-induced treatment, a significant number of ssDNA molecules are released below 37 °C. Achieving ssDNA release at or near 37 °C (physiological temperature) is particularly important for avoiding hyperthermic cell death.[45,46] In all measurements summarized in Figure 1, the error bars were within the symbols used to plot the data, however, significant batch-to-batch variations most likely due to

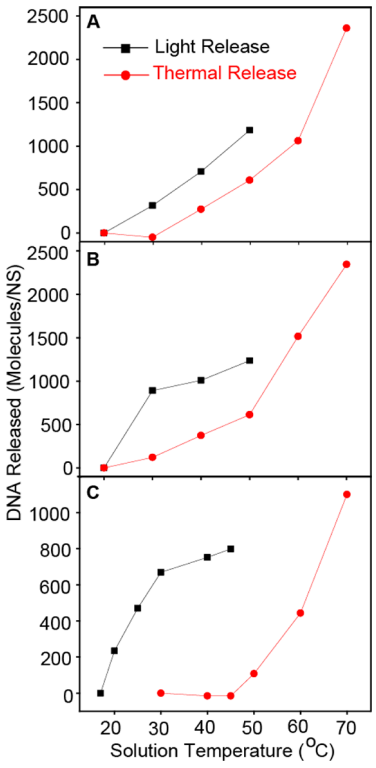

Figure 1. Thermal and laser-triggered release of ssDNA from Au nanoshell-PLL vector. Thermal release (red circles) and light release (black squares) of (A) short ssDNA (18 bases), (B) phosphorothioate-modified short ssDNA (18 bases), and (C) long ssDNA (50 bases).

the uncertainty in number of nanoparticles, number of host molecules, density-dependent crowding effects, and the number of releasable cargo molecules, were present and are characteristic of these types of systems.[36]

The difference between purely thermal and light-induced release profiles does not necessarily reflect a difference in release mechanism. For light-induced release, the localized heating around each nanoshell results in a nonuniform thermal profile and the macroscopic solution temperature does not reflect the temperature at the illuminated nanoshell surface. Localized heating in the direct, nanoscale vicinity around the nanoshell could release the ssDNA prior to increasing the ambient solution temperature. Additional nonthermal mechanisms may likely be involved, such as photon-induced transfer of "hot" electrons, generated by laser excitation, to the poly-L-lysine peptide. This would reduce the electrostatic interaction between the poly-L-lysine and ssDNA and enable release with little or no temperature increase of the local environment.[36]

We compare the total number of DNA molecules attached to a PLL-functionalized nanoshell, termed "loading capacity", to the number of ssDNA molecules released from a nanoshell during the thermal and light release processes (Table 2). The loading capacity was

TABLE 2. Quantification of ssDNA Loading Capacity and Release[a]

	loading capacity (DNA/nanoshell)	light release (DNA/nanoshell)	thermal release (DNA/nanoshell)
short ssDNA	3050	1182	2357
phosphorothioate-modified short ssDNA	8182	1236	2345
long ssDNA	3189	799	1097

[a] Number of DNA released per nanoshell at highest recorded solution temperature.

determined by a previously reported method (see methods, Supporting Information).[36,47] The phosphorothioate-modified short ssDNA has a much higher loading capacity (8182 DNA molecule/nanoshell) compared to the short ssDNA (3050 DNA molecules/nanoshell), even though the DNA base composition and sequence length are identical (Table 1). This could be a result of the phosphorothioate modification, which replaces a nonbridging oxygen in the phosphate backbone with a sulfur atom. These additional sulfur atoms may potentially bind to the Au surface of the nanoshells, increasing the loading capacity of this molecule. Despite its greater loading capacity, the number of molecules released per nanoshell is strikingly similar for both the phosphorothioate-modified short ssDNA (thermal release, 2345 DNA/nanoshell; light release, 1236 DNA/nanoshell) and the chemically unmodified short ssDNA (thermal release, 2357 DNA/nanoshell; light release, 1182 DNA/nanoshell). This also suggests that some of the phosphorothioate-modified ssDNA strands are covalently attached to the Au surface through the sulfur group in the phosphorothioate modification, preventing its release under these conditions. Only the electrostatically associated oligonucleotides are released for the light-induced and the thermally induced treatments in these experiments. It is also important to note that we saw no evidence of release of the PLL host from the nanoparticles in these experiments.

Since the interaction between the ssDNA and PLL is predominantly electrostatic, the length of the DNA sequence should affect the profile of the release. Shorter oligonucleotide sequences should interact less strongly with PLL and thus be released at lower temperatures. To validate this hypothesis, we compared the release profiles of short (18 bases) and long (50 bases) ssDNA (Table 1). For the thermal process, the short ssDNA begins to release between 30 and 40 °C (Figure 1A), while the long ssDNA begins to release between 40 and 50 °C (Figure 1C). For the light-induced process, both the short and the long ssDNAs are released at a lower solution temperature relative to the thermal treatments. The number of long ssDNA molecules released per NS (~800) is significantly lower than the number of short ssDNA molecules released per NS (~1180) although the loading capacities of the

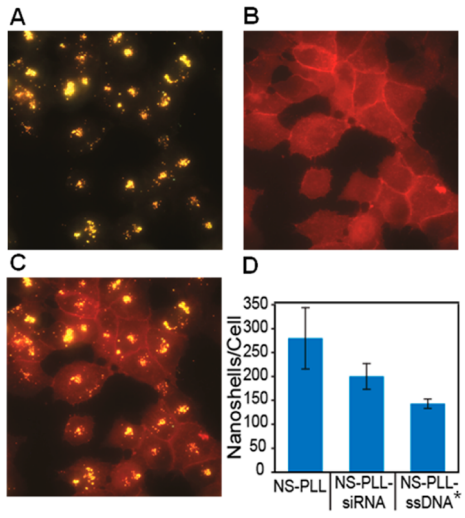

Figure 2. Cell uptake of NS-PLL delivery vectors in H1299 cells. (A–C) Dark-field/fluorescence images showing (A) poly-L-lysine nanoshells (NS-PLL), (B) cell membrane stained red with Alexa Fluor 555 WGA, and (C) images A and B merged together showing poly-L-lysine nanoshells uptaken in cells. (D) Quantification of the number of nanoshells per cell determined by inductively coupled plasma mass spectrometry (ICP–MS) after a I_2/KI gold etch procedure. Error bars represent standard deviations (n = 5).

two sequences are similar (3200 molecules/NS) (Table 2). This is expected due to the increase in electrostatic interactions between the long ssDNA and PLL. These measurements were performed at the same ambient temperature with the same laser exposure time. Therefore, by varying the length of the poly-L-lysine and ssDNA, it should be possible to control the number of ssDNA molecules released into the system while keeping all other conditions constant.

Cellular Uptake of Nanoshell-Poly-L-lysine Delivery Vectors. For effective delivery of antisense oligonucleotides and siRNA, the NS-PLL delivery vector must be uptaken within the cell and escape the endosome. To facilitate cell uptake, the NS-PLL was incubated with H1299 cells for 2 h in serum-containing cell culture medium. After incubation, the cells were either fixed and cellular uptake was investigated using dark-field microscopy (Figure 2A) and fluorescence microscopy (Figure 2B), or the number of nanoshells uptaken per cell was quantified by inductively coupled plasma mass spectrometry (Figure 2D). Nanoshells of this size both absorb and scatter light, making them easily visible in dark-field microscopy as diffraction-limited bright spots (Figure 2A). The cell membrane is marked by the red fluorescence dye, Alexa Fluor 555 WGA (wheat germ agglutinin). Figure 2C shows the merged dark-field and fluorescence images demonstrating the colocalization of NS-PLL within cells.

Since neither dark-field nor fluorescence microscopy can definitively determine whether nanoshells are endocytosed or remain outside the cell but associate with the cell membrane, ICP–MS was used to confirm and quantify nanoshell cellular uptake. Uptake was quantified in H1299 cells respectively treated with three NS-PLL constructs: (1) poly-L-lysine nanoshells (NS-PLL), (2) poly-L-lysine nanoshells with phosphorothioate-modified short ssDNA electrostatically attached (NS-PLL-ssDNA), and (3) poly-L-lysine nanoshells with siRNA electrostatically attached (NS-PLL-siRNA). After a 12 h incubation of these constructs, the media was aspirated off and the cells were washed twice with phosphate buffered saline. To eliminate noninternalized nanoshells, an iodine/potassium iodide (I_2/KI) etchant procedure was performed[41] (see methods, Supporting Information). The etchant rapidly oxidizes any gold at the exterior of the cell membrane, and is nontoxic at low concentrations. Using this method with ICP–MS, we detected that 277 ± 64 NS-PLL per cell, 198 ± 28 NS-PLL-siRNA per cell, and 141 ± 10 NS-PLL-ssDNA per cell were internalized in H1299 cells, respectively (Figure 2D). In principle, combining the measurement of the number of internalized nanoparticles with the light-induced release profile can enable us to determine the number of oligonucleotides delivered within the cell.

TABLE 3. ζ-Potential Measurements

sample	surface potential (mV)
nanoshells (NS)	−23.23 ± 3.9
NS-PLL	14.27 ± 3.6
NS-PLL-siRNA	10.74 ± 2.2
NS-PLL-ssDNA[a]	0.28 ± 4.4

[a] Phosphorothioate-modified short ssDNA. Error represents standard deviations (n = 5).

While repeating experiments to confirm reproducibility, the number of nanoshells uptaken was observed to vary among different samples. We hypothesized that the cellular uptake depended on the surface charge of the poly-L-lysine nanoshell delivery vectors. To investigate, we measured the zeta (ζ)-potential for each sample (Table 3). A control sample of bare nanoshells has a negative ζ-potential (−23.23 ± 3.9 mV). Attachment of PLL to the NSs results in a net positive ζ-potential (14.27 ± 3.6 mV). After attachment of the negatively charged siRNA or ssDNA, the ζ-potential decreased accordingly. Interestingly, the ssDNA causes a significantly larger decrease (0.28 ± 4.41 mV), indicating that a greater number of ssDNA molecules was attached to the NS-PLL compared to double-stranded siRNA molecules (10.74 ± 2.2 mV). This was expected due to the higher affinity of the phosphorothioate-modified ssDNA to the NS-PLL complex. There is also a significant difference in the conformation between single-stranded DNA and double-stranded siRNA, which could possibly allow more of the smaller ssDNA sequences to bind to the poly-L-lysine compared to the larger double-stranded siRNA.

The highest cellular uptake was recorded with the NS-PLL sample with the highest positive ζ-potential, while the lowest cellular uptake was obtained for NS-PLL-ssDNA with the lowest ζ-potential. This correlation between net positive charge of the particle and uptake highlights the importance of carrier surface chemistry to the uptake mechanism.

Previous studies regarding the uptake of cationic peptides, polymers, and nanoparticles suggest an adsorptive endocytosis pathway.[48−51] First, the positively charged poly-L-lysine-functionalized nanoshells adsorb onto the negatively charged cell membrane surface and are then internalized *via* endocytosis. It was recently shown that adsorption of particles to the cell membrane is the rate-limiting step for this mechanism.[41] Because the NS-PLL sample has the greatest positive charge, this is likely to increase its interactions with the cell surface and reduce the time needed for adsorption. Therefore, a greater number of the NS-PLL particles are adsorbed onto the cell membrane and ultimately internalized.[41]

Downregulation of Green Fluorescence Protein *in Vitro*. To study the ability of the NS-PLL delivery vector to release RNAi therapeutic oligonucleotides *in vitro*, fluorescence microscopy was used to visualize the release of fluorescently tagged ssDNA from NS-PLL within the H1299 lung cancer cells. The NS-PLL-ssDNA sample was incubated with H1299 cells in an identical procedure as the cell uptake studies presented earlier. The ssDNA was tagged on the 5′ end with Alexa Fluor 488, a green fluorophore. After the 2 h incubation, the media was removed by aspiration and replaced with fresh media. Half of the cells do not undergo a laser treatment (Figure 3A) and the other half are irradiated with a laser treatment, 2.5 W/cm^2 for 2 min (Figure 3B). Finally, the cells are fixed and the cell membrane is stained red by Alexa Fluor 555 WGA. Figure 3A shows that without laser treatment the green fluorescence is very weak, most likely because the Alexa Fluor 488 fluorescence is quenched due to the proximity of the ssDNA to the gold nanoshell surface. In Figure 3B, the laser treatment results in an increased brightness of the green fluorescence because the ssDNA is released from the NS-PLL delivery vector, which eliminates the quenching. Additionally, in the laser treatment group, it appears that the green fluorescence is more delocalized throughout the cell, indicating that the DNA may have escaped from the endosome. Further confocal imaging experiments are warranted to give definitive information regarding endosomal escape. Our imaging results do not show definitively whether the endocytosed nanocomplexes are sequestered within endosomes or free within the cytosol.[52,53]

The rupturing of the endosome in response to laser irradiation has been the subject of intense recent research.[54−56] The light-controlled disruption is dependent on both the laser intensity and time of laser

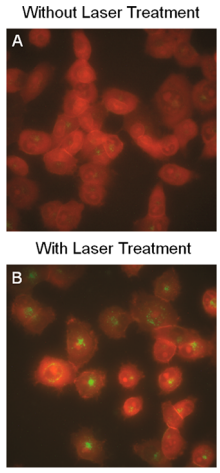

Figure 3. Fluorescence images H1299 cells incubated with NS-PLL-ssDNA. The ssDNA is fluorescently tagged with Alexa Fluor 488 (green). (A) Without laser treatment, the green fluorescence is quenched because of the proximity of the ssDNA to the gold nanoshell surface. (B) With laser treatment, the ssDNA is released, which eliminates the quenching, resulting in brighter green fluorescence spread throughout the cell.

irradiation. For both high continuous wave (CW) laser intensity (~10^5 W/cm^2) and pulsed laser irradiation conditions, the photothermal properties of the nanoparticle result in the heating of the surrounding environment leading to endosomal membrane disruption.[55] For low CW laser intensity irradiation conditions, like the conditions used within this study (2.5 W/cm^2 for 2 min), the increase in temperature is minimal, suggesting the possibility of a nonthermal, photochemical mechanism.[36,57] Krpetić *et al*., recently showed that lower laser irradiation powers (<20 W/cm^2 for 2 min) resulted in a minimal temperature increase and significant endosome damage, and concluded that by controlling both laser power and exposure time, highly selective, localized damage could be inflicted on the endosomal membrane without inducing cell death.[54] Escape of the molecular payload from the endosome, by whatever mechanism, is required for the therapeutic oligonucleotides to be effective.

To investigate the effectiveness of our NS-PLL delivery vector to deliver RNAi therapeutic oligonucleotides which downregulate a protein, a lung cancer cell line (H1299-dsGFP/dsRFP) that expresses destabilized green fluorescent protein (GFP) and destabilized red fluorescent protein (RFP) was used. Destabilized fluorescent proteins were chosen because they have short half-lives that allow for the monitoring of downregulation shortly after administration of the molecular therapeutics.[58−60] The GFP was used as the target reporter for determining downregulation of gene and protein expression by phosphorothioate-modified single-stranded antisense DNA oligonucleotide (AON-GFP) or siRNA specific to GFP mRNA (siRNA-GFP). The RFP served as a reference protein to ensure accurate

measurements of GFP despite variations in fluorescence intensity due to variations in cell number. This was achieved by designing the siRNA and antisense oligos to downregulate GFP without affecting the RFP. Thus, for all measurements, the peak fluorescence intensity of GFP was normalized by the peak intensity of RFP (GFP/RFP).[60]

Three separate poly-L-lysine nanoshell complexes were prepared: NS-PLL, NS-PLL-siRNA, and NS-PLL-ssDNA. Here, the ssDNA was identical to the phosphorothioate-modified short ssDNA used in the extracellular release studies described earlier. The antisense oligonucleotides and siRNA sequences used in these experiments were chosen from previous studies and have been previously investigated for specificity[59,61,62] and, furthermore, were compared to scrambled sequences to ensure specific downregulation of GFP (Figure S2, Supporting Information).

The downregulation of GFP by antisense oligonucleotides (Figure 4A) and siRNA (Figure 4B) delivered *via* NS-PLL delivery vectors was monitored by measuring the peak fluorescence intensity of both GFP and RFP at specific time points: prior to incubation (0 h), after incubation and prior to laser treatment (12 h), and after laser treatment (15, 18, 24, and 36 h). The laser treatment for the NS-PLL sample, which had neither siRNA nor ssDNA attached, resulted in negligible GFP downregulation (Figure 4C, NS-PLL). In Figure 3A,B, the "with laser" and "without laser" are normalized percentages to the "with laser" and "without laser" of the NS-PLL sample, respectively. During the incubation period (0−12 h), GFP expression was downregulated by antisense ssDNA to 72 ± 5% (Figure 4A) and by siRNA to 80 ± 5% (Figure 4B). This downregulation was likely due to the AON-GFP and siRNA-GFP weakly bound to the PLL which came off the delivery vector during cell incubation. At 12 h, half of the cells were irradiated with the laser for 2 min. At 18 h, six hours after laser treatment, GFP downregulation for the laser-treated samples had reached its minimum (~47% for antisense ssDNA and ~49% for siRNA, Figure 4C). Therefore, the laser-treated samples resulted in an additional ~23% and ~31% GFP downregulation for antisense ssDNA and siRNA, respectively, when compared to the non-laser treated samples. This difference in downregulation indicates that the laser treatment controllably released the gene therapeutics from the NS-PLL delivery vector. The samples not treated with the laser showed no further downregulation after the incubation period. In fact, GFP expression increased shortly after incubation, indicating that the initial downregulation observed during incubation was limited to the ssDNA or siRNA released during the 12 h incubation. We anticipate that optimizing the NS-PLL incubation time would either minimize or reduce the downregulation observed before laser treatment. Because GFP is continuously produced and expressed within the cell,

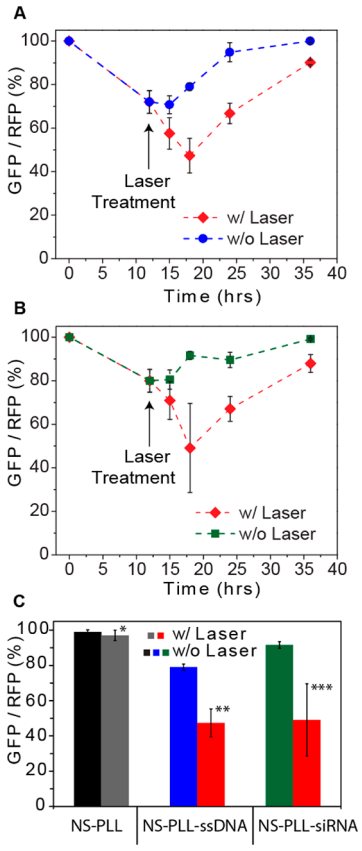

Figure 4. Downregulation of green fluorescent protein (GFP) in H1299 GFP/RFP cell line by antisense ssDNA and siRNA using nanoshell poly-L-lysine (NS-PLL) delivery vectors. (A,B) Percent GFP/RFP fluorescence as a function of time with and without laser treatment for NS-PLL delivery vectors carrying with (A) antisense ssDNA and (B) siRNA. (C) Percent GFP/RFP fluorescence at 18 h (6 h after laser treatment). Data displayed as mean ± SEM ($n = 3$). Unpaired *t* tests: (*) $P = 0.5934$, (**) $P = 0.0176$, (***) $P = 0.1071$.

after the ssDNA or siRNA is consumed, the GFP/RFP percentage gradually increases, approaching its pretreatment value after 24 h following laser irradiation.

The observed magnitude of the downregulation of GFP is similar for both delivery vectors, despite their difference in ζ-potential. The data in Table 3 suggests that fewer siRNA molecules are attached to the NS-PLL delivery vector compared to antisense ssDNA, because the NS-PLL-siRNA sample has a higher positive ζ-potential. However, Figure 4C shows that both samples had ~50% downregulation of GFP when treated with the laser. This observation correlates well with studies showing that siRNA is more efficient in silencing genes and downregulating their protein expression relative to phosphorothioate-modified antisense ssDNA.[42,59] Interestingly, we observed a greater downregulation of GFP for light-triggered release of RNAi oligonucleotides when the cells were trypsinized prior to laser treatment compared to adhered cells (data not shown). Any effect that this trypsin procedure would have on protein expression is negated because the GFP downregulation data shown in Figure 3 is normalized to

the NS-PLL group that also underwent the trypsin procedure.

From a kinetic point of view, GFP downregulation reaches its maximum at approximately 6 h after laser treatment. This time frame for observing GFP downregulation is consistent with both experimental and theoretical results that used antisense oligonucleotides and siRNA to downregulate short half-life destabilized proteins.[58−60] Additionally, the light-triggered delivery process is significantly different from traditional passive transfection reagents such as liposomes and dendrimers. With a transfection reagent, the delivery of the RNAi oligonucleotides occurs over multiple hours, if not days, because these RNAi oligonucleotides must slowly escape the endosome, dissociate from the transfection reagent, and finally diffuse to the mRNA in the cytosol. In the case of light-triggered delivery, the vast majority of the oligonucelotides is released during the short laser irradiation treatment (2 min). Therefore, it is likely that the gene silencing and the subsequent protein expression downregulation occurs faster due to the higher initial concentration of released RNAi oligonucleotides in the cytosol of cells. Further studies would be needed to determine if light-induced processes, or combinations of light-controlled processes, could be used to more generally modify cellular processes in this manner.

In estimating the amount of therapeutic RNAi oligonucleotides delivered, we hypothesize that the percentage of the RNAi oligonucleotides released intracellularly is similar to the extracellular release, in which a maximum of ~1200 ssDNA were released per nanoshell. This hypothesis is theorized since the laser radiation takes place within the "water window," where water and tissue are maximally transparent, such that the cellular environment should have a minimal effect on the NS response to laser irradiation.[29] Additionally, the release of the RNAi oligonucleotides is due to either the local heat generated around the nanoshell or the generation of hot electrons on the gold surface, neither of which should be affected by the cellular environment.[36] If this hypothesis is correct, by using the ICP−MS nanoshell uptake result for NS-PLL-ssDNA (~141 nanoshells/cell) and the number of ssDNA released extracellularly below 37 °C (~1000 ssDNA/NS), then a maximum of ~141 000 antisense oligonucleotides would be released inside the cell. After converting this number to moles and dividing by the intracellular volume (4×10^{-12} L),[58,63] we can estimate that ~60 nM of antisense oligonucleotides are delivered inside each cell *via* light-triggered release from the NS-PLL vector. This approximate concentration correlates well to the ~50% GFP downregulation we observed, according to both previously reported experimental results and theoretical models.[58,59,64] Although this is an approximation, it points to future capabilities for delivering known amounts of therapeutic molecules using vectors such as our poly-L-lysine nanoshell complex at specific time points, to study the kinetics of physical, chemical, and biological processes within live cells. The efficiency of the poly-L-lysine nanoshell delivery vector demonstrated here can be improved by increasing the intracellular uptake, optimizing laser irradiation conditions, and the integration of targeting moieties for studies *in vivo*.

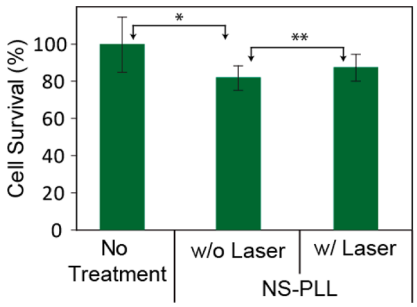

Figure 5. Analysis of NS-PLL nanoparticle-associated cytotoxicity by XTT assay. Percent survival of H1299 cells with no treatment compared to cells incubated with nanoshell−poly-L-lysine (NS-PLL) delivery vector without laser treatment (w/o Laser) and with laser treatment (w/Laser), mean ± standard deviation ($n = 3$). Unpaired *t* tests: (*) $P = 0.1237$, (**) $P = 0.3747$.

Cell Viability Assay. The cell viability of the H1299-GFP/RFP cell line after incubation with the poly-L-lysine nanoshell delivery vectors and subsequent laser treatment was investigated by using a XTT assay (Figure 5). Incubation of the nanoshell-poly-L-lysine delivery vectors with no laser treatment resulted in 82 ± 6% cell survival. After laser irradiation, there was 88 ± 7% cell survival, indicating that the laser treatment is not detrimental to the cells. This may come as a surprise considering Au nanoshells are well-known for photothermal cancer therapy, but the laser power and exposure time used in this study (2.5 W/cm^2, 2 min) were significantly less than those used for photothermal induction of cell death (4W/cm^2, 3−6 min).[30,31,34,46] The NS-PLL sample was chosen for cell viability because this sample had the greatest uptake of nanoshells, and therefore it would have had the greatest possibility to cause photothermal cell death. The small decrease in the percent of cell survival in the nonirradiated sample could possibly result from a variety of factors, including the ζ-potential of this sample or free poly-L-lysine that is not attached to the nanoshell.[65] Additionally, nanoparticle concentration and incubation time have been shown to affect cell viability.[66] Cationic transfection reagents that show low toxicity are often linked with polyethylene glycol (PEG), which reduces toxicity without affecting transfection efficiency, but attachment of PEG to our NS-PLL platform has yet to be investigated.

CONCLUSIONS

In this work, we have quantitatively demonstrated the remotely controlled, light-triggered release of antisense ssDNA from poly-L-lysine nanoshell vectors. The cellular uptake of the NS-PLL complex in H1299 lung cancer cells was investigated by fluorescence microscopy, dark-field microscopy, and ICP–MS. This poly-L-lysine nanoshell complex was successfully used as a nonviral delivery vector that could controllably release antisense oligonucleotide ssDNA and siRNA to silence the target reporter GFP gene and downregulate GFP protein expression *in vitro*. Neither the poly-L-lysine nanoshells nor the laser treatment showed any significant evidence of cytotoxicity, indicating that this nanoparticle complex could further be used to quantify the number of molecules delivered intracellularly, which could have extensive applications in studying the rates of specific processes within living cells.

METHODS

Nanoshell Synthesis and Poly-L-lysine Functionalization. Au nanoshells were synthesized according to a previously published method.[28] The dimensions of the silica core and the Au shell ($[r_1, r_2]$ = [60, 82] nm) were designed so that the peak plasmon resonance in an aqueous suspension occurred at 800 nm, corresponding to the laser excitation wavelength used in this experiment (Figure S1, Supporting Information). The concentration of nanoshells in water is determined by the following equation which is derived from Beer's law:

$$\frac{\text{nanoshells}}{\text{mL}} = \frac{2.303 x A_{\text{peak}}}{\sigma_{\text{ext}} x b}$$

where A_{peak} = experimental absorption at the peak plasmon resonance wavelength, σ_{ext} = theoretical extinction cross section at the peak plasmon resonance wavelength taken from Mie theory, and b = path length of the cuvette in centimeters.

Poly-L-lysine Attachment to Nanoshells. The cysteine (C)–tyrosine (Y)–serine (S)–lysine(K)$_{50}$ (PLL) peptide was custom synthesized (Biomatik USA, LLC). The peptide was received as a lyophilized powder and resuspended in Milli-Q water to a concentration of 500 μM. Once the concentration of nanoshells is known, this PLL peptide is added to the solution of nanoshells in 100,000 molar excess of PLL. This solution was allowed to incubate for 24 h on a rocker at room temperature. The excess PLL was removed *via* two centrifugation cycles (350 rcf for 15 min) and resuspended in Milli-Q water. ζ-Potential measurements confirmed PLL attachment (Table 3).

ssDNA or siRNA Loading. Antisense ssDNA and siRNA were custom synthesized by Integrated DNA technologies (IDT) and Qiagen, respectively. ssDNA and siRNA was resuspended in TE buffer and nuclease-free water, respectively, to a final concentration of ~100 μM. A 50,000 molar excess of ssDNA or siRNA was added to the Au NS-PLL suspension previously prepared and allowed to incubate for 24 h on a rocker at room temperature. The nanoshell solution was placed in the refrigerator at 4 °C and allowed to gently settle down for 48 h. Afterward, the supernatant was pipetted off and the pellet was resuspended in Milli-Q water. (Note: For the fluorescein-tagged-ssDNA release experiments, resuspension in TE buffer (IDT, pH = 7.5) is necessary to ensure that the pH is constant since the emission properties of fluorescein are pH dependent.)

Loading Capacity of Fluorescently Tagged ssDNA on the NS-PLL Vector. Two aliquots of 500 uL of NS-PLL-ssDNA were pipettes into two separate 1.5 mL eppindorf tubes. In one tube, 500 uL of TE buffer was added and in the other tube 500 uL of 12 mM mercaptoethanol (diluted in TE buffer) was added. Both tubes were covered in aluminum foil and were gently mixed on a rocker plate for 24 h. Mercaptoethanol displaces the poly-L-lysine and ssDNA attached to the nanoshell. After 24 h, both samples were centrifuged to remove the nanoshells, then the supernatants were measured in a fluorolog (excitation wavelength: 495 nm, emission wavelengths: 505–540 nm). The difference in fluorolog intensity between samples was used to calculate the difference in DNA concentration by using a standard curve of DNA concentration *versus* fluorescence intensity. The DNA concentration was then divided by the nanoshell concentration, which is calculated by UV–vis absorbance measurement.

Thermal and Light-Triggered Release of ssDNA. Thermal release was performed by slowly heating the NS-PLL-ssDNA sample (~1 °C/min) while stirring, ensuring that the sample temperature was homogeneous during the entire course of the measurement. The light release was performed by placing a fiber-coupled 800 nm continuous wave laser above the sample and stirring during laser irradiation. For both thermal and laser treatments, the solution temperature was monitored with a thermocouple. The release of the fluorescently tagged ssDNA was quantified by taking aliquots out of the sample as the solution temperature increased. Each aliquot was centrifuged immediately to separate the nanoshells from the released ssDNA in the supernatant and the fluorescence intensity of the supernatant was measured to determine the number of released ssDNA per nanoshell.

Cell Culture. The H1299 and H1299-GFP/RFP lung cancer cell lines were incubated at 5% CO_2, 37 °C with RPMI 1640 media with L-glutamine supplemented with 10% heat-inactivated fetal bovine serum and 1% antibiotic solution. Trypsin-EDTA (0.25%) was used for cell passaging.

NS-PLL Cellular Uptake. The H1299-GFP/RFP lung cancer cells were seeded in 4-well chamber slides at 5000 cells/well 24 h prior to incubation with NS-PLL delivery vectors. The nanoshells were added to the serum containing media in a NS/cell ratio of 5000:1 and allowed to incubate for 2 h. Then, the cell culture medium was aspirated off, the cells were washed twice with 1× phosphate buffered saline and the cells were fixed with 4% paraformaldehyde and stained with Alexa Fluor 555 according to manufacturer instructions. The walls of the chamber slide were removed, and the cells were mounted using Vectashield mounting medium for fluorescence (Vector Laboratories) and 22 mm × 50 mm rectangular cover glass (n = 1.5). Dark-field and fluorescence images were taken on a Cytoviva microscope equipped with dual-mode fluorescence module and a x-cite light source. For quantification of nanoshells uptaken in cells, ICP–MS measurements were performed. After a 12 h incubation, the media was aspirated off, the cells were washed twice with PBS and the I_2/KI etchant procedure was perfomed (see methods, Supporting Information). Live cells were sorted and counted using flow cytometry and digested with aqua regia, and then the gold content was measured with the ICP–MS (see methods, Supporting Information).

Fluorescence Images for Light-Triggered Release. NS-PLL-ssDNA delivery vectors were incubated with cells in an identical manner to NS-PLL uptake. The ssDNA is fluorescently tagged with Alexa Fluor 488 (Integrated DNA technologies, IDT) After 2 h, the media was aspirated off, the cells were washed twice with 1× phosphate buffered saline and fresh media was added. The laser treatment group under went a laser treatment (2.5 W/cm^2, 2 min). Immediately afterward, the media was aspirated off, fixed, and stained in an identical procedure as the NS-PLL cellular uptake experiments and imaged with a Cytoviva microscope.

Laser Treatment for GFP Downregulation. H1299-GFP/RFP cells were plated in a 12-well plate at a density of 95000 cells/well 12 h before incubation with NS-PLL, NS-PLL-ssDNA, and NS-PLL-siRNA delivery vectors. These NS-PLL delivery vectors were incubated with cells in an identical manner as the NS-PLL cell uptake experiments. After incubation the cell culture media was

aspirated of, the cells were washed with PBS, trypsinized, and resupsended in cell culture media. Half of each cell suspension was irradiated with an 800 nm CW laser for 2 min at 2.5 W/cm^2 and the other half did not undergo laser irradiation. The cells are then plated back onto a fresh 24 well plate. Green fluorescence protein (GFP) and red fluorescence protein (RFP) were measured at specific time points using a fluorescence plate reader.

XTT Assay. After the laser treatment the cells were allowed to grow for 12 h, and then the XTT assay (sodium 2,3,-bis(2-methoxy-4-nitro-5-sulfophenyl)-5-[(phenylamino)-carbonyl]-2*H*-tetrazolium inner salt) was performed according to XTT kit instructions (ATCC).

Conflict of Interest: The authors declare no competing financial interest.

Acknowledgment. This work was supported by the Robert A. Welch Foundation (C-1220, Halas), Alliance for Nanohealth (W81XWH-09-2-0139, Ji and Halas), a NIH/NCI Specialized Program of Research Excellence (SPORE) (CA-070907, Minna and Roth), and a R01 (CA-116322, Ji). We thank The University of Texas MD Anderson Cancer Center South Campus Flow Cytometry Core Lab funded by a NCI Cancer Center Support Grant (No. P30CA16672). We thank M. Jebb for help with ICP–MS. We thank D. Zhang and O. Neumann for many helpful discussions.

Supporting Information Available: Characterization of silica core–Au shell nanoshells. (Figure S1); Dharmafect control experiment (Figure S2); Histogram of nanoshell size (Figure S3), and extensive materials and methods section. This material is available free of charge *via* the Internet at http://pubs.acs.org.

REFERENCES AND NOTES

1. Elbashir, S. M.; Harborth, J.; Lendeckel, W.; Yalcin, A.; Weber, K.; Tuschl, T. Duplexes of 21-Nucleotide RNAs Mediate RNA Interference in Cultured Mammalian Cells. *Nature* **2001**, *411*, 494–498.
2. Soutschek, J.; Akinc, A.; Bramlage, B.; Charisse, K.; Constien, R.; Donoghue, M.; Elbashir, S.; Geick, A.; Hadwiger, P.; Harborth, J.; *et al*. Therapeutic Silencing of an Endogenous Gene by Systemic Administration of Modified SiRNAs. *Nature* **2004**, *432*, 173–178.
3. de Fougerolles, A.; Vornlocher, H.-P.; Maraganore, J.; Lieberman, J. Interfering With Disease: A Progress Report on siRNA-Based Therapeutics. *Nat. Rev. Drug Discovery* **2007**, *6*, 443–453.
4. Devi, G. R. siRNA-Based Approaches in Cancer Therapy. *Cancer Gene Ther.* **2006**, *13*, 819–829.
5. Kim, D. H.; Rossi, J. J. Strategies For Silencing Human Disease Using RNA Interference. *Nat. Rev. Genet.* **2007**, *8*, 173–184.
6. Zimmermann, T. S.; Lee, A. C. H.; Akinc, A.; Bramlage, B.; Bumcrot, D.; Fedoruk, M. N.; Harborth, J.; Heyes, J. A.; Jeffs, L. B.; John, M.; *et al*. RNAi-Mediated Gene Silencing in Non-human Primates. *Nature* **2006**, *441*, 111–114.
7. John, M.; Constien, R.; Akinc, A.; Goldberg, M.; Moon, Y.-A.; Spranger, M.; Hadwiger, P.; Soutschek, J.; Vornlocher, H.-P.; Manoharan, M.; *et al*. Effective RNAi-Mediated Gene Silencing without Interruption of the Endogenous MicroRNA Pathway. *Nature* **2007**, *449*, 745–U12.
8. Davis, M. E.; Zuckerman, J. E.; Choi, C. H. J.; Seligson, D.; Tolcher, A.; Alabi, C. A.; Yen, Y.; Heidel, J. D.; Ribas, A. Evidence of RNAi in Humans From Systemically Administered siRNA *via* Targeted Nanoparticles. *Nature* **2010**, *464*, 1067–1070.
9. Luo, D.; Saltzman, W. M. Synthetic DNA Delivery Systems. *Nat. Biotechnol.* **2000**, *18*, 33–37.
10. Mintzer, M. A.; Simanek, E. E. Nonviral Vectors for Gene Delivery. *Chem. Rev.* **2009**, *109*, 259–302.
11. Elsabahy, M.; Nazarali, A.; Foldvari, M. Non-viral Nucleic Acid Delivery: Key Challenges and Future Directions. *Curr. Drug Delivery* **2011**, *8*, 235–244.
12. Taratula, O.; Garbuzenko, O. B.; Kirkpatrick, P.; Pandya, I.; Savla, R.; Pozharov, V. P.; He, H. X.; Minko, T. Surface-Engineered Targeted PPI Dendrimer for Efficient Intracellular and Intratumoral siRNA Delivery. *J. Controlled Release* **2009**, *140*, 284–293.
13. Lu, W.; Zhang, G.; Zhang, R.; Flores, L. G.; Huang, Q.; Gelovani, J. G.; Li, C. Tumor Site–Specific Silencing of NF-κB p65 by Targeted Hollow Gold Nanosphere–Mediated Photothermal Transfection. *Cancer Res.* **2010**, *70*, 3177–3188.
14. Morille, M.; Passirani, C.; Vonarbourg, A.; Clavreul, A.; Benoit, J.-P. Progress in Developing Cationic Vectors for Non-viral Systemic Gene Therapy against Cancer. *Biomaterials* **2008**, *29*, 3477–3496.
15. Jin, S.; Ye, K. M. Nanoparticle-Mediated Drug Delivery and Gene Therapy. *Biotechnol. Prog.* **2007**, *23*, 32–41.
16. Duncan, B.; Kim, C.; Rotello, V. M. Gold Nanoparticle Platforms as Drug and Biomacromolecule Delivery Systems. *J. Controlled Release* **2010**, *148*, 122–127.
17. Ganta, S.; Devalapally, H.; Shahiwala, A.; Amiji, M. A Review of Stimuli-Responsive Nanocarriers for Drug and Gene Delivery. *J. Controlled Release* **2008**, *126*, 187–204.
18. Wijaya, A.; Schaffer, S. B.; Pallares, I. G.; Hamad-Schifferli, K. Selective Release of Multiple DNA Oligonucleotides from Gold Nanorods. *ACS Nano* **2009**, *3*, 80–86.
19. Chen, C. C.; Lin, Y. P.; Wang, C. W.; Tzeng, H. C.; Wu, C. H.; Chen, Y. C.; Chen, C. P.; Chen, L. C.; Wu, Y. C. DNA-Gold Nanorod Conjugates for Remote Control of Localized Gene Expression by Near Infrared Irradiation. *J. Am. Chem. Soc.* **2006**, *128*, 3709–3715.
20. Barhoumi, A.; Huschka, R.; Bardhan, R.; Knight, M. W.; Halas, N. J. Light-Induced Release of DNA from Plasmon-Resonant Nanoparticles: Towards Light-Controlled Gene Therapy. *Chem. Phys. Lett.* **2009**, *482*, 171–179.
21. Ghosh, P.; Han, G.; De, M.; Kim, C. K.; Rotello, V. M. Gold Nanoparticles in Delivery Applications. *Adv. Drug Delivery Rev.* **2008**, *60*, 1307–1315.
22. Braun, G. B.; Pallaoro, A.; Wu, G. H.; Missirlis, D.; Zasadzinski, J. A.; Tirrell, M.; Reich, N. O. Laser-Activated Gene Silencing *via* Gold Nanoshell-siRNA Conjugates. *ACS Nano* **2009**, *3*, 2007–2015.
23. Takahashi, H.; Niidome, Y.; Yamada, S. Controlled Release of Plasmid DNA from Gold Nanorods Induced by Pulsed Near-Infrared Light. *Chem. Commun.* **2005**, *17*, 2247–2249.
24. Yamashita, S.; Fukushima, H.; Akiyama, Y.; Niidome, Y.; Mori, T.; Katayama, Y.; Niidome, T. Controlled-Release System of Single-Stranded DNA Triggered by the Photothermal Effect of Gold Nanorods and its *in Vivo* Application. *Bioorg. Med. Chem.* **2011**, *19*, 2130–2135.
25. Poon, L.; Zandberg, W.; Hsiao, D.; Erno, Z.; Sen, D.; Gates, B. D.; Branda, N. R. Photothermal Release of Single-Stranded DNA from the Surface of Gold Nanoparticles through Controlled Denaturating and Au-S Bond Breaking. *ACS Nano* **2010**, *4*, 6395–6403.
26. Jones, M. R.; Millstone, J. E.; Giljohann, D. A.; Seferos, D. S.; Young, K. L.; Mirkin, C. A. Plasmonically Controlled Nucleic Acid Dehybridization with Gold Nanoprisms. *Chemphyschem* **2009**, *10*, 1461–1465.
27. Lee, S. E.; Liu, G. L.; Kim, F.; Lee, L. P. Remote Optical Switch for Localized and Selective Control of Gene Interference. *Nano Lett.* **2009**, *9*, 562–570.
28. Oldenburg, S. J.; Averitt, R. D.; Westcott, S. L.; Halas, N. J. Nanoengineering of Optical Resonances. *Chem. Phys. Lett.* **1998**, *288*, 243–247.
29. Weissleder, R. A Clearer Vision for *in Vivo* Imaging. *Nat. Biotechnol.* **2001**, *19*, 316–317.
30. Stern, J. M.; Stanfield, J.; Kabbani, W.; Hsieh, J.-T.; Cadeddu, J. A. Selective Prostate Cancer Thermal Ablation with Laser Activated Gold Nanoshells. *J. Urology* **2008**, *179*, 748–753.
31. Gobin, A. M.; Lee, M. H.; Halas, N. J.; James, W. D.; Drezek, R. A.; West, J. L. Near-Infrared Resonant Nanoshells for Combined Optical Imaging and Photothermal Cancer Therapy. *Nano Lett.* **2007**, *7*, 1929–1934.
32. Lal, S.; Clare, S. E.; Halas, N. J. Nanoshell-Enabled Photothermal Cancer Therapy: Impending Clinical Impact. *Acc. Chem. Res.* **2008**, *41*, 1842–1851.
33. Bardhan, R.; Chen, W. X.; Perez-Torres, C.; Bartels, M.; Huschka, R. M.; Zhao, L. L.; Morosan, E.; Pautler, R. G.; Joshi, A.; Halas, N. J. Nanoshells with Targeted Simultaneous Enhancement of Magnetic and Optical Imaging and

Photothermal Therapeutic Response. *Adv. Funct. Mater* **2009**, *19*, 3901–3909.
34. O'Neal, D. P.; Hirsch, L. R.; Halas, N. J.; Payne, J. D.; West, J. L. Photo-thermal Tumor Ablation in Mice Using Near Infrared-Absorbing Nanoparticles. *Cancer Lett.* **2004**, *209*, 171–176.
35. Murphy, C. J.; Gole, A. M.; Stone, J. W.; Sisco, P. N.; Alkilany, A. M.; Goldsmith, E. C.; Baxter, S. C. Gold Nanoparticles in Biology: Beyond Toxicity to Cellular Imaging. *Acc. Chem. Res.* **2008**, *41*, 1721–1730.
36. Huschka, R.; Zuloaga, J.; Knight, M. W.; Brown, L. V.; Nordlander, P.; Halas, N. J. Light-Induced Release of DNA from Gold Nanoparticles: Nanoshells and Nanorods. *J. Am. Chem. Soc.* **2011**, *133*, 12247–12255.
37. Huschka, R.; Neumann, O.; Barhoumi, A.; Halas, N. J. Visualizing Light-Triggered Release of Molecules Inside Living Cells. *Nano Lett.* **2010**, *10*, 4117–4122.
38. Choi, Y. H.; Liu, F.; Kim, J. S.; Choi, Y. K.; Park, J. S.; Kim, S. W. Polyethylene Glycol-grafted Poly-L-lysine as Polymeric Gene Carrier. *J. Controlled Release* **1998**, *54*, 39–48.
39. Ghosh, P. S.; Kim, C. K.; Han, G.; Forbes, N. S.; Rotello, V. M. Efficient Gene Delivery Vectors by Tuning the Surface Charge Density of Amino Acid-Functionalized Gold Nanoparticles. *ACS Nano* **2008**, *2*, 2213–2218.
40. Han, S.; Mahato, R. I.; Sung, Y. K.; Kim, S. W. Development of Biomaterials for Gene Therapy. *Mol. Ther.* **2000**, *2*, 302–317.
41. Cho, E. C.; Xie, J.; Wurm, P. A.; Xia, Y. Understanding the Role of Surface Charges in Cellular Adsorption *versus* Internalization by Selectively Removing Gold Nanoparticles on the Cell Surface with a I2/KI Etchant. *Nano Lett.* **2009**, *9*, 1080–1084.
42. Grunweller, A.; Wyszko, E.; Bieber, B.; Jahnel, R.; Erdmann, V. A.; Kurreck, J. Comparison of Different Antisense Strategies in Mammalian Cells using Locked Nucleic Acids, 2′-*O*-Methyl RNA, Phosphorothioates and Small Interfering RNA. *Nucleic Acids Res.* **2003**, *31*, 3185–3193.
43. Agrawal, S.; Temsamani, J.; Tang, J. Y. Pharmokinetics, Biodistribution, and Stability of Oligodeoxynucleotide Phosphorothioates in Mice. *Proc. Natl. Acad. Sci. U.S.A.* **1991**, *88*, 7595–7599.
44. Neurath, M. F.; Pettersson, S.; Zum Büschenfelde, K. H. M.; Strober, W. Local Administration of Antisense Phosphorothioate Oligonucleotides to the p65 Subunit of NF-kappa B Abrogates Established Experimental Colitis in Mice. *Nat. Med.* **1996**, *2*, 998–1004.
45. Huang, X. H.; Jain, P. K.; El-Sayed, I. H.; El-Sayed, M. A. Determination of the Minimum Temperature Required for Selective Photothermal Destruction of Cancer Cells with the use of Immunotargeted Gold Nanoparticles. *Photochem. Photobiol.* **2006**, *82*, 412–417.
46. Hirsch, L. R.; Stafford, R. J.; Bankson, J. A.; Sershen, S. R.; Rivera, B.; Price, R. E.; Hazle, J. D.; Halas, N. J.; West, J. L. Nanoshell-Mediated Near-Infrared Thermal Therapy of Tumors under Magnetic Resonance Guidance. *Proc. Natl. Acad. Sci. U.S.A.* **2003**, *100*, 13549–13554.
47. Demers, L. M.; Mirkin, C. A.; Mucic, R. C.; Reynolds, R. A.; Letsinger, R. L.; Elghanian, R.; Viswanadham, G. A Fluorescence-Based Method for Determining the Surface Coverage and Hybridization Efficiency of Thiol-Capped Oligonucleotides Bound to Gold Thin Films and Nanoparticles. *Anal. Chem.* **2000**, *72*, 5535–5541.
48. Zauner, W.; Ogris, M.; Wagner, E. Polylysine-based Transfection Systems Utilizing Receptor-Mediated Delivery. *Adv. Drug Delivery Rev.* **1998**, *30*, 97–113.
49. Shen, W. C.; Ryser, H. J. P. Conjugation of Poly-L-Lysine to Albumin and Horseradish-Peroxidase—Novel Method of Enhancing Cellular Uptake of Proteins. *Proc. Natl. Acad. Sci. U.S.A.* **1978**, *75*, 1872–1876.
50. Ryser, H. J. P.; Drummond, I.; Shen, W. C. The Cellular Uptake of Horseradish-Peroxidase and its Poly(lysine) Conjugate by Cultured Fibroblasts Is Qualitatively Similar Despite a 900-Fold Difference in Rate. *J. Cell. Physiol.* **1982**, *113*, 167–178.
51. Leonetti, J.-P.; Degols, G.; Lebleu, B. Biological Activity of Oligonucleotide-Poly(L-lysine) Conjugates: Mechanism of Cell Uptake. *Bioconjugate Chem.* **1990**, *1*, 149–153.
52. Verma, A.; Uzun, O.; Hu, Y. H.; Hu, Y.; Han, H. S.; Watson, N.; Chen, S. L.; Irvine, D. J.; Stellacci, F. Surface-Structure-Regulated Cell-Membrane Penetration by Monolayer-Protected Nanoparticles. *Nat. Mater.* **2008**, *7*, 588–595.
53. Xu, L. G.; Kuang, H.; Xu, C. L.; Ma, W.; Wang, L. B.; Kotov, N. A. Regiospecific Plasmonic Assemblies for *in Situ* Raman Spectroscopy in Live Cells. *J. Am. Chem. Soc.* **2012**, *134*, 1699–1709.
54. Krpetic, Z. E.; Nativo, P.; See, V.; Prior, I. A.; Brust, M.; Volk, M. Inflicting Controlled Nonthermal Damage to Subcellular Structures by Laser-Activated Gold Nanoparticles. *Nano Lett.* **2010**, *10*, 4549–4554.
55. Carregal-Romero, S.; Ochs, M.; Rivera-Gil, P.; Ganas, C.; Pavlov, A. M.; Sukhorukov, G. B.; Parak, W. J. NIR-Light Triggered Delivery of Macromolecules into the Cytosol. *J. Controlled Release* **2012**, *159*, 120–127.
56. Lukianova-Hleb, E. Y.; Belyanin, A.; Kashinath, S.; Wu, X.; Lapotko, D. O. Plasmonic Nanobubble-Enhanced Endosomal Escape Processes for Selective and Guided Intracellular Delivery of Chemotherapy to Drug-Resistant Cancer Cells. *Biomaterials* **2012**, *33*, 1821–1826.
57. Govorov, A. O.; Richardson, H. H. Generating Heat with Metal Nanoparticles. *Nano Today* **2007**, *2*, 30–38.
58. Bartlett, D. W.; Davis, M. E. Insights into the Kinetics of siRNA-Mediated Gene Silencing from Live-Cell and Live-Animal Bioluminescent Imaging. *Nucleic Acids Res.* **2006**, *34*, 322–333.
59. Bertrand, J. R.; Pottier, M.; Vekris, A.; Opolon, P.; Maksimenko, A.; Malvy, C. Comparison of Antisense Oligonucleotides and siRNAs in Cell Culture and *in Vivo*. *Biochem. Biophys. Res. Commun.* **2002**, *296*, 1000–1004.
60. Eguchi, A.; Meade, B. R.; Chang, Y. C.; Fredrickson, C. T.; Willert, K.; Puri, N.; Dowdy, S. F. Efficient siRNA Delivery into Primary Cells by a Peptide Transduction Domain-dsRNA Binding Domain Fusion Protein. *Nat. Biotechnol.* **2009**, *27*, 567–571.
61. Kim, S. H.; Mok, H.; Jeong, J. H.; Kim, S. W.; Park, T. G. Comparative Evaluation of Target-Specific GFP Gene Silencing Efficiencies for Antisense ODN, Synthetic siRNA, and siRNA Plasmid Complexed with PEI-PEG-FOL Conjugate. *Bioconjugate Chem.* **2006**, *17*, 241–244.
62. Rosi, N. L.; Giljohann, D. A.; Thaxton, C. S.; Lytton-Jean, A. K. R.; Han, M. S.; Mirkin, C. A. Oligonucleotide-Modified Gold Nanoparticles for Intracellular Gene Regulation. *Science* **2006**, *312*, 1027–1030.
63. Chiu, D. T.; Zare, R. N. Assaying for Peptides in Individual Aplysia Neurons with Mass Spectrometry. *Proc. Natl. Acad. Sci. U.S.A.* **1998**, *95*, 3338–3340.
64. Bartlett, D. W.; Davis, M. E. Effect of siRNA Nuclease Stability on the *in Vitro* and *in Vivo* Kinetics of siRNA-Mediated Gene Silencing. *Biotechnol. Bioeng.* **2007**, *97*, 909–921.
65. Lv, H. T.; Zhang, S. B.; Wang, B.; Cui, S. H.; Yan, J. Toxicity of Cationic Lipids and Cationic Polymers in Gene Delivery. *J. Controlled Release* **2006**, *114*, 100–109.
66. Fischer, D.; Li, Y. X.; Ahlemeyer, B.; Krieglstein, J.; Kissel, T. *In Vitro* Cytotoxicity Testing of Polycations: Influence of Polymer Structure on Cell Viability and Hemolysis. *Biomaterials* **2003**, *24*, 1121–1131.